

Reduction of Energy Deposition Non-Uniformity by Adjustment of Pellet Structure for Heavy-Ion-Beam Inertial Confinement Fusion^{*)}

Zhehao LIN, Kazumasa TAKAHASHI, Toru SASAKI and Takashi KIKUCHI

Nagaoka University of Technology, Nagaoka 940-2188, Japan

(Received 10 January 2022 / Accepted 23 March 2022)

We herein propose a fuel pellet with a flower-shaped tamper and an ablator layer filled with a heavier material as a heavy-ion inertial fusion target. The proposed fuel pellet structure successfully mitigates the non-uniformity of energy deposition owing to the different penetration depths at different parts of the incident heavy-ion beams. The heavier material in the ablator interferes with the movement of the ablator material. The low-density region in the ablator layer at the edge of the irradiated area is mitigated, and direct heating of the fuel by heavy-ion beams is prevented.

© 2022 The Japan Society of Plasma Science and Nuclear Fusion Research

Keywords: direct drive, heavy-ion-beam, inertial confinement fusion, preheating, tamper

DOI: 10.1585/pfr.17.2404064

1. Introduction

Heavy-ion beam inertial confinement fusion (HIF) is a promising thermonuclear fusion energy source [1]. Although almost all proposals for the HIF system are based on an indirect drive scheme from the viewpoint of beam-lines in the HIF accelerator complex and hydrodynamic stability, a direct-indirect hybrid target scheme has the advantage of coexistence for irradiation uniformity and pellet gain [2]. Non-uniformity is a key issue in HIF [3–5] and laser-driven inertial confinement fusion [6, 7]. In a massive-ion beam driver system [8], the direct irradiation of fuel pellets with multi-bunch ion beams is feasible. However, the irradiation uniformity of the incident ion beams remains limited. The non-uniformity of implosion due to non-uniform irradiation is a significant issue in HIF occurring in massive-ion beam driver systems. A fuel pellet structure typically comprises fuel and an ablator. In direct-driven HIF, because the heavy-ion beam (HIB) deposits a major part of the energy at the end of its stopping range, a tamper layer is added to the outer layer of the ablator to increase the implosion efficiency [9].

Non-uniform energy deposition causes non-uniform pressure distribution in the ablator area. The pressure gradient from the high- to low-energy deposition area causes changes in the density distribution of the ablator and tamper. This results in a non-uniform mass density distribution of the tamper and ablator. Consequently, the energy deposition profile of the HIBs changes, and the irradiation non-uniformity increases. We herein propose a fuel pellet structure with a flower-shaped tamper to mitigate this issue. The penetration length of the HIBs adjusts the tamper shape in the fuel pellet, and the non-uniformity of the HIB

irradiation is mitigated. In addition, a heavier material is used to fill the ablator layer, thereby disrupting the lateral movement of the ablator material. Consequently, the preheating of the fuel is mitigated by a flower-shaped tamper with a heavier material-filled structure.

2. Governing Equation and Calculation Condition

In this study, we developed a two-dimensional hydrodynamic code in cylindrical coordinates using the CIP (constrained interpolation profile) [10] and MmB (local maximum and minimum bounds) [11] methods based on a two-temperature ideal gas and Euler coordinates to investigate the tamper effect in ICF target implosion. The calculation grid configuration was set at 300×300 points. Artificial viscosity was used [12], and a splitting model [13] was applied. Ionization was calculated using the Saha equation [14]. The governing equations are as follows:

$$\frac{\partial \rho}{\partial t} + \frac{1}{r} \frac{\partial (r \rho u_r)}{\partial r} + \frac{\partial (\rho u_z)}{\partial z} = 0 \quad (1)$$

$$\frac{\partial u_r}{\partial t} + u_r \frac{\partial u_r}{\partial r} + u_z \frac{\partial u_r}{\partial z} + \frac{1}{\rho} \frac{\partial (P_i + P_e + Q_{ir} + Q_{er})}{\partial r} = 0$$

$$\frac{\partial u_z}{\partial t} + u_r \frac{\partial u_z}{\partial r} + u_z \frac{\partial u_z}{\partial z} + \frac{1}{\rho} \frac{\partial (P_i + P_e + Q_{iz} + Q_{ez})}{\partial z} = 0 \quad (2)$$

$$\left(\frac{\partial T_i}{\partial t} + u_r \frac{\partial T_i}{\partial r} + u_z \frac{\partial T_i}{\partial z} \right) + \frac{P_i}{\rho C v_i} \left(\frac{1}{r} \frac{\partial r u_r}{\partial r} + \frac{\partial u_z}{\partial z} \right)$$

$$+ \frac{1}{\rho C v_i} \left(Q_{ir} \frac{1}{r} \frac{\partial r u_r}{\partial r} + Q_{iz} \frac{\partial u_z}{\partial z} \right)$$

$$+ \omega_{ie} (T_i - T_e) = 0$$

$$\left(\frac{\partial T_e}{\partial t} + u_r \frac{\partial T_e}{\partial r} + u_z \frac{\partial T_e}{\partial z} \right) + \frac{P_e}{\rho C v_e} \left(\frac{1}{r} \frac{\partial r u_r}{\partial r} + \frac{\partial u_z}{\partial z} \right)$$

author's e-mail: s195084@stn.nagaokaut.ac.jp

^{*)} This article is based on the presentation at the 30th International Toki Conference on Plasma and Fusion Research (ITC30).

$$\begin{aligned}
 & + \frac{1}{\rho C v_e} \left(Q_{er} \frac{1}{r} \frac{\partial r u_r}{\partial r} + Q_{ez} \frac{\partial u_z}{\partial z} \right) - \frac{\omega_{ie}}{Z_{\text{eff}}} (T_i - T_e) \\
 & = \frac{\Delta E_{\text{free}} + \Delta E_{\text{bound}}}{\rho C v_e \Delta V}.
 \end{aligned} \quad (3)$$

Here, ρ is the density; T_i and T_e are the temperatures of ions and electrons, respectively; Q_{ir} and Q_{iz} are the artificial viscosities of ions in the r - and z -directions, respectively; Q_{er} and Q_{ez} are the artificial viscosities of electrons in the r - and z -directions, respectively; $C v_i$ and $C v_e$ are the ion and electron specific heats, respectively; P_i and P_e are the ion and electron pressures, respectively; ω_{ie} is the ion-electron collision frequency; Z_{eff} is the effective charge of the ion; ΔE_{free} and ΔE_{bound} are the deposition energies to free and bound electrons, respectively; and ΔV is the cell volume.

The energy deposition scheme in this study is based on the Bethe–Bloch and LSS theories for bound electrons and the Jackson binary and collective theory for free electrons [15].

3. Fuel Pellet Structure and Irradiation Configuration

In this study, we designed two types of pellet structures. The thickness difference of the tamper between the different regions of the incident HIB causes energy deposition non-uniformity, as shown in Fig. 1.

The first type is a pellet structure with a flower-shaped tamper for mitigating non-uniformity, as shown in Fig. 2. In the first structure type, the midpoint of each petal of the tamper is fixed, and the radius of curvature R of the tamper petal can be varied to obtain the optimal configuration, as shown in Fig. 2. Incident HIBs are indicated by the shaded red areas shown in Fig. 2. When $R = 4.07$ mm, the tamper and fuel pellet are concentric spheres, i.e., the tamper is a conventional spherical tamper. We selected lead as the tampering material, aluminum as the ablator material, and a mixture of D (deuterium) and T (tritium) as the fuel. The entire structure remained at 300 K (Kelvin) before HIB irradiation.

The second type of pellet structure is designed to mitigate non-uniformity from the lateral movement of the ablator material caused by the pressure gradient between the irradiated and unirradiated areas, as shown in Fig. 3. Inci-

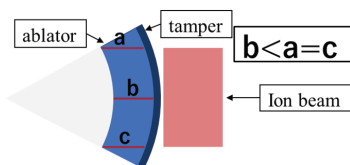


Fig. 1 HIB irradiating target with tamper layer. At the edge of the incident HIB, the thickness of the tamper is a or c , whereas that at the center of the incident HIB is c , and $b < a = c$.

dent HIBs are indicated by the shaded red areas shown in Fig. 3. The second type resembles the first type in terms of pellet structure. The unirradiated area in the ablator layer was filled with a tamper material. The boundary of the filled material remained parallel to the edge of the irradiated area. The angle θ between the boundaries of the filling material can be varied to determine the optimal configuration, as shown in Fig. 3. When $\theta = 0.0^\circ$, the tamper material filled the entire unirradiated area, without the filling material, into the irradiated area in the ablator.

Hereinafter, the fuel pellet (first type) shown in Fig. 2 is referred to as the “non-filled pellet,” and the fuel pellet (second type) shown in Fig. 3 is referred to as the “filled pellet.”

The ions in the HIBs were Pb^+ with 11.4 GeV of energy. We set the kinetic energy to 11.4 GeV for the point of the Bragg peak near the inner edge of the ablator layer. To

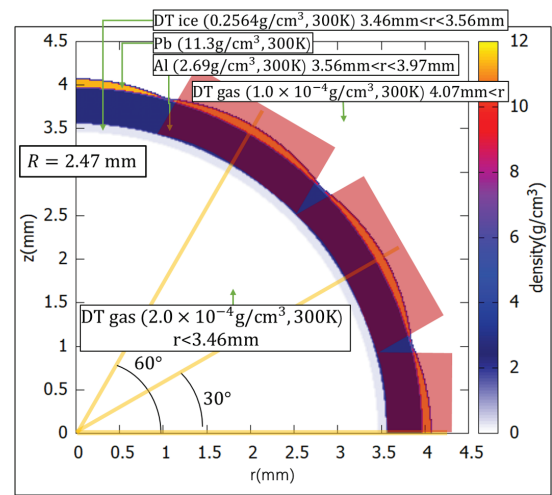


Fig. 2 First type of pellet structure (non-filled pellet) with flower-shaped tamper.

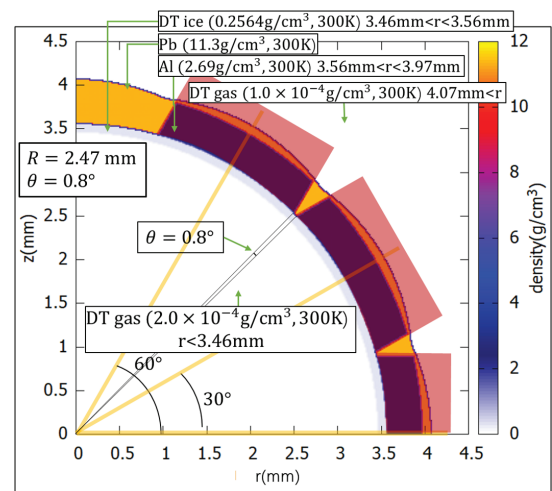


Fig. 3 Second type of pellet structure (filled pellet) with flower-shaped tamper and a region of ablator filled by tamper material.

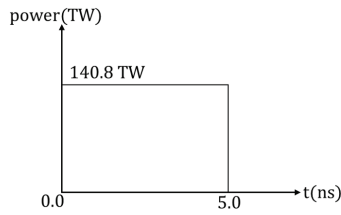


Fig. 4 Power of total incident HIBs.

cover the fuel pellet, 44 beams were required, except for the polar area, as shown in Figs. 2 and 3. The density of the HIBs was uniformly distributed in the radial direction, and the beam radius was 0.92 mm. The total irradiation power was 140.8 TW, and the total energy of the HIBs was 0.704 MJ. The total power history of the HIBs is shown in Fig. 4. The pulse duration was 5 ns. The beam current and power per beam were 280 A and 3.2 TW, respectively.

4. Results

The density distributions at 1.5 ns for the non-filled pellet with tamper petal radii R of 4.07 mm (conventional spherical tamper) and 3.87 mm are shown in Fig. 5. The energy depositions by incident HIBs at 1.5 ns for the non-filled pellet with tamper petal radii R of 4.07 and 3.87 mm are shown in Fig. 6 in which the gray area represents the DT fuel layer. The electron and ion temperature distributions at 1.5 ns for the non-filled pellet with tamper petal radii R of 4.07 mm (conventional spherical tamper) and 3.87 mm are shown in Figs. 7 and 8, respectively. In Fig. 5, in the area indicated by the red arrow, the case for $R = 3.87$ mm, shows a higher uniformity compared with $R = 4.07$ mm (conventional spherical tamper). However, in the cases where $R = 3.87$ mm and $R = 4.07$ mm, the fuel was preheated at the edge of the irradiation area, as shown in the area indicated by the red arrow in Fig. 6. Because the flower-shaped tamper adjusted the penetration depth of the HIBs in the fuel pellet, the non-uniformity of the deposition energy was mitigated around the Bragg peak position. At the Bragg peak position, the energy deposition exhibited a profile without overlapping beams or non-irradiated regions. However, the non-irradiated region of the HIBs occurred in the area from the fuel pellet surface to the Bragg peak position, as indicated by the green arrow in Fig. 6. The pressure gradient in the ablator was generated between the irradiated and non-irradiated areas. The pressure gradient caused the lateral movement of the ablator material, and the density distribution in the ablator changed owing to the pressure gradient. The lateral movement of the ablator created a low-density region at the edge of the irradiated area. The area indicated by the green arrow in Fig. 5 indicates a low-density path at the edge of the irradiated area. Therefore, the HIB has a relatively long stopping range at the edge of the irradiated area. Consequently, the fuel is directly heated by the HIBs passing through the low-density region in the ablator. This phenomenon is not ob-

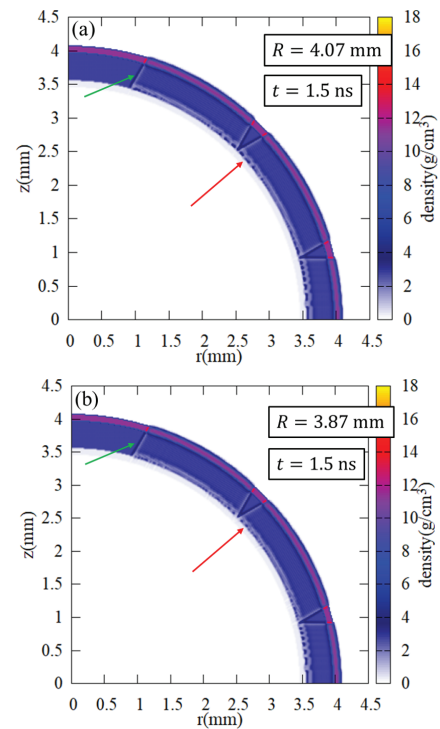


Fig. 5 Density distribution at 1.5 ns for non-filled pellet with tamper petal radius R (a) of 4.07 mm and (b) 3.87 mm.

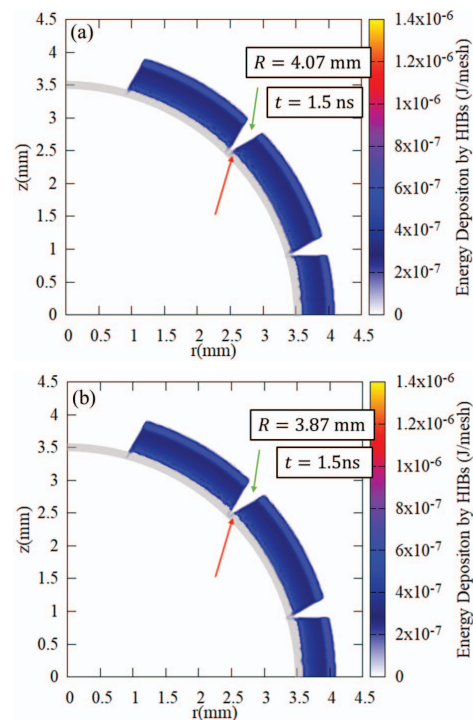


Fig. 6 Energy distribution by HIBs at 1.5 ns for non-filled pellet with tamper petal radius R (a) of 4.07 mm and (b) 3.87 mm.

served in the early stage, as shown in Fig. 9, which shows the density distribution and energy deposition by the incident HIBs at 0.5 ns of the same fuel pellet (Fig. 5 (a)). The movement of the ablator material was insufficient to create

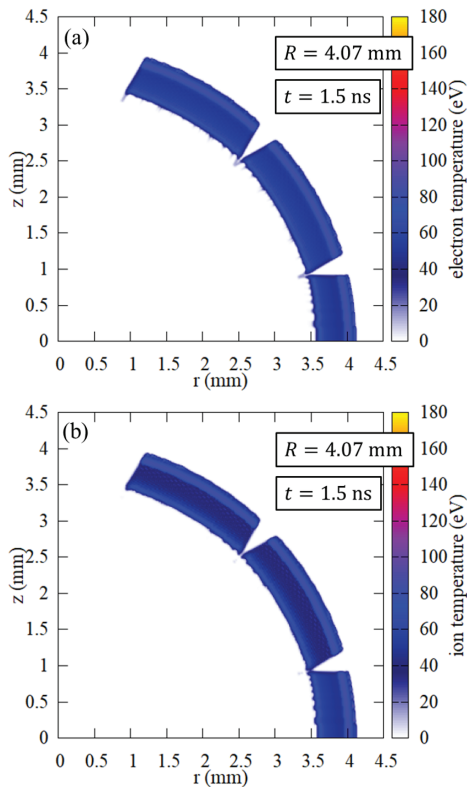


Fig. 7 Electron and ion temperature distributions at 1.5 ns for non-filled pellet with tamper petal radius R of 4.07 mm. (a) Electron temperature; (b) ion temperature.

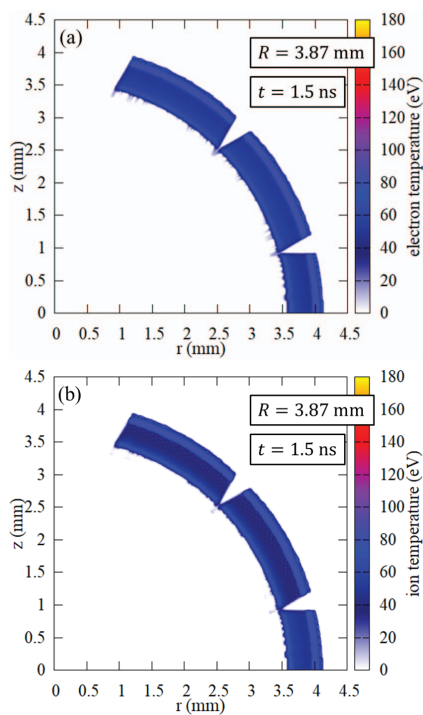


Fig. 8 Electron and ion temperature distributions at 1.5 ns for non-filled pellet with tamper petal radius R of 3.87 mm. (a) Electron temperature; (b) ion temperature.

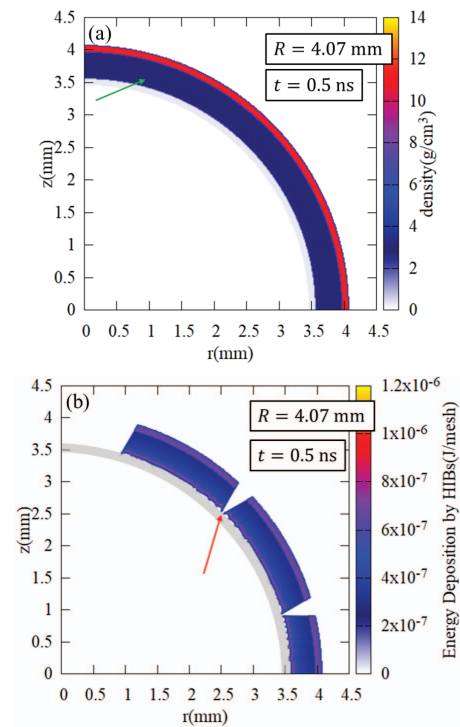


Fig. 9 Density and energy deposition distributions by HIB irradiation at 0.5 ns for non-filled pellet with tamper petal radius R of 4.07 mm. (a) Density; (b) energy deposition.

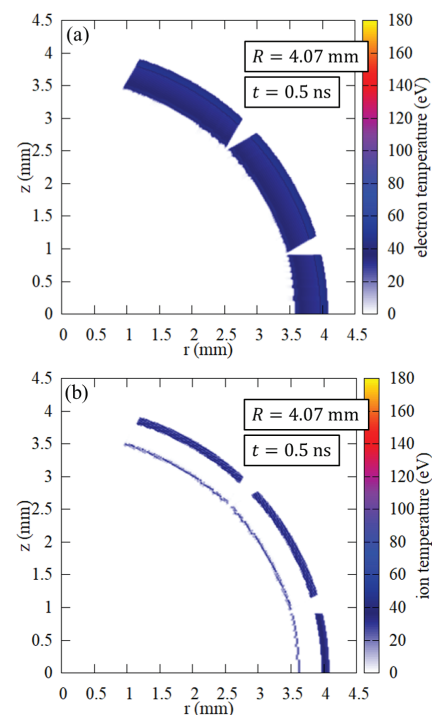


Fig. 10 Electron and ion temperature distributions at 0.5 ns for non-filled pellet with tamper petal radius R of 4.07 mm. (a) Electron temperature; (b) ion temperature.

a low-density region (the area indicated by the green arrow in Fig. 9 (a)). The corresponding electron and ion temperature distributions are shown in Fig. 10. Consequently, the

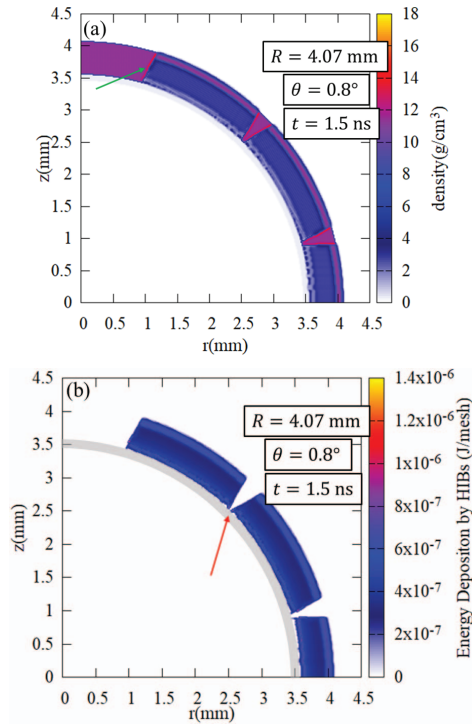


Fig. 11 Density and energy deposition distributions by HIB irradiation at 1.5 ns for filled pellet with tamper petal radius R of 4.07 mm and angle parameter $\theta = 0.8^\circ$. (a) Density; (b) energy deposition.

Bragg peak position of the HIBs did not shift into the fuel layer, as shown in Fig. 9 (b).

To mitigate non-uniformity, we propose a second type of pellet structure. The density distribution and energy deposition by incident HIBs at 1.5 ns of the filled pellet with a tamper petal radius R of 4.07 mm and an angle parameter $\theta = 0.8^\circ$ are shown in Figs. 11 (a) and (b), where the gray area in Fig. 11 (b) represents the DT fuel layer. The filling material is heavier than the ablator material. In this case, the ablator material is Al, and the tamper and filling materials are Pb. Hence, although the ablator pressure in the irradiated area increased owing to the heating by the HIB energy deposition, the filled material interfered with the lateral movement of the ablator owing to the pressure gradient. The low-density region at the edge of the irradiated area is mitigated, as shown by the green arrows in Fig. 8 (a). Consequently, the preheating of the fuel is mitigated, as shown in Fig. 8 (b). The corresponding electron and ion temperature distributions are shown in Fig. 12. The fuel temperature did not increase because of the energy deposition of the HIBs, as the Bragg peak position was in the ablator.

5. Conclusion

We proposed a fuel pellet with a flower-shaped tamper (a non-filled pellet) and successfully mitigated the non-uniformity of energy deposition caused by different pene-

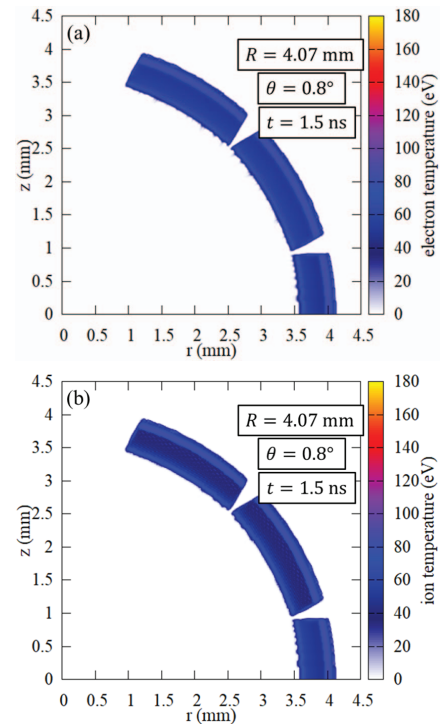


Fig. 12 Electron and ion temperature distributions at 1.5 ns for filled pellet with tamper petal radius R of 4.07 mm and angle parameter $\theta = 0.8^\circ$. (a) Electron temperature; (b) ion temperature.

tration depths at different parts of incident HIBs. At the early time, the energy deposition profile of the HIBs was uniform at the Bragg peaks. However, the non-irradiated region of the HIBs occurred in the area from the fuel pellet surface to the Bragg peak position. The pressure gradient between the irradiated and non-irradiated regions caused the ablator to move and created low-density regions at the edge of the irradiated region in the ablator layer. Consequently, the HIBs possessed a longer stopping range in the low-density regions, and the Bragg peak position of the HIBs shifted into the fuel layer. Subsequently, the fuel temperature increased owing to direct heating by the HIBs. It is noteworthy that fuel preheating is undesirable.

To mitigate the issue above, we proposed a fuel pellet with an ablator layer filled with a heavier material in the non-irradiated region (filled pellet). The heavier material in the ablator interfered with the movement of the ablator material. The low-density region at the edge of the irradiated area was mitigated, and the HIBs had the same penetration length as in the ablator layer. Consequently, the direct heating of fuel by HIBs was mitigated. The fuel pellet structure proposed herein was demonstrated to be suitable for uniform HIB irradiation and implosion to achieve higher fuel compression in HIF.

In future studies, implosion dynamics will be investigated based on the proposed configuration of fuel pellets.

- [1] K. Horioka, *Matter Radiat. Extremes* **3**, 12 (2018).
- [2] Y. Iizuka *et al.*, *J. Plasma Fusion Res. Series* **8**, 1200 (2009).
- [3] A.I. Ogoyski *et al.*, *Phys. Lett. A* **315**, 372 (2003).
- [4] T. Someya *et al.*, *Phys. Rev. Accel. Beams* **7**, 044701 (2004).
- [5] S. Miyazawa *et al.*, *Phys. Plasmas* **12**, 122702 (2005).
- [6] S. Skupsky and K. Lee, *J. Appl. Phys.* **54**, 3662 (1983).
- [7] M. Murakami *et al.*, *Phys. Plasmas* **17**, 082702 (2010).
- [8] K. Takayama *et al.*, *Phys. Lett. A* **384**, 126692 (2020).
- [9] S. Kawata, *Adv. Phys.: X* **6**, 1873860 (2021).
- [10] T. Yabe, *J. Comput. Phys.* **169**, 556 (2001).
- [11] H. Wu and S. Yang, *IMPACT of Computing in Science and Engineering* **1**, 217 (1989).
- [12] V.F. Kuropatenko, *Amer. Math. Soc.*, Providence, 116 (1967).
- [13] D.S. Miller, *Comput. Fluids* **210**, 104672 (2020).
- [14] J.W. Fowler, <https://arxiv.org/abs/1209.1111>
- [15] T.A. Mehlhorn, *J. Appl. Phys.* **52**, 6522 (1981).